JST: Engineering and Technology for Sustainable Development
Volume 34, Issue 4, October 2024, 040-047

Detection of Nitrofurantoin Antibiotic via Electrochemical Technique Using Green Synthesized Iron/Graphene/Tetrakis (4-Carboxyphenyl) Porphyrin Nanocomposite as Electrode Material

Nguyen Thi Xuan Quynh[1], Cao Hong Ha[1], La Duc Duong[2], Dang Trung Dung[1*]
[1]School of Chemistry and Life Sciences, Hanoi University of Science and Technology, Ha Noi, Vietnam
[2]Institute of Chemistry and Materials, Academy of Military Science and Technology, Ha Noi, Vietnam
[*]Corresponding author email: dung.dangtrung@hust.edu.vn

Abstract

Antibiotic residues are always a threat to human health. Nitrofurantoin (NFT) is an antibiotic commonly used in agriculture, which can be dangerous to human life when entering the body through antibiotic residues in food. The green synthesized iron/graphene nanocomposite has shown promising electrochemical properties as a sensor for detecting NFTs. The morphology and structure of iron/graphene nanocomposite materials were evaluated by modern analyses, including Scanning Electron Microscope combined with Energy Dispersive X-ray Spectroscopy elemental mapping (SEM-EDX mapping) and Fourier-transform infrared spectroscopy (FT-IR). The results show that iron nanoparticles with a size of 30-50 nm are evenly distributed on the graphene surface and interspersed in the porphyrin fibers. The factors of scan rate, pH, and amount of material affecting the ability to identify NFT in solution were investigated. A standard plot with a wide linear range of 1-200 µM was built to analyze NFT antibiotics. The results open up the potential for applying Fe/GNPs nanocomposite materials in electrochemical sensors to detect residues of other antibiotics in food.

Keywords: Green synthesis, electrochemical sensor, Nitrofurantoin.

1. Introduction

Cancer is always the top health concern for humanity. According to GLOBOCAN statistics in its 2020 report, the number of cases and deaths due to cancer in the world and Vietnam, in particular, tends to increase. Out of the 185 participating countries, Vietnam ranked 90th in the number of new cancer cases and 50th in the number of cancer deaths. Causes of cancer are divided into two main sources: factors that cannot be changed (age, genes,...) and factors that are amendable (lifestyle, environment,...) [1]. One of the changeable causes is the consumption of foods containing antibiotic residue exceeding the allowable level [2]. Moreover, it leads to the development of antibiotic resistance in both humans and animals, negatively affects the environment, and creates challenges in exporting agricultural products. Nitrofurantoin (NFT) has the chemical formula $C_8H_6N_4O_5$ and is widely used as a feed additive in livestock and aquaculture to prevent and treat bacterial infections and protozoa, as well as promote their growth. Many studies have found that NFT has the potential to be toxic to the liver and cause birth defects [3]. Therefore, it is imperative to manage the utilization of NFT in agriculture strictly, as well as to have convenient, yet effective, measurements to detect antibiotic residues.

With the continuous development of materials science, electrochemical methods are increasingly prominent because of their superiority to conventional solutions. Electrochemical sensors allow for quick, convenient analysis without requiring highly skilled technicians. Furthermore, they provide rapid determination of analytes with high sensitivity, a low detection limit, and a wide working range. Therefore, this method offers flexibility and ease of operation in the field. Currently, there are four types of materials utilized in electrochemical sensors: metal nanomaterials, metal oxide nanomaterials, carbon nanomaterials, and metal-organic frameworks, of which metallic nanomaterials are the most common [4]. Among them, iron is a good conductive metal and is much cheaper than gold, silver, platinum, or cerium. In addition, iron nanoparticles can be easily synthesized by many processes, especially from green chemistry with the input chemicals being Cleistocalyx Operculatus (CO) extract and iron (III) salt, which allows reduced production costs, and is friendly to environment [5]. Currently, there has been research on immobilizing zero-valent iron nanomaterials on polymer nanofibers to synthesize nanocomposite materials for catalysis and sensing applications, which yielded highly promising results [6]. Zero-valent iron nanoparticles (Fe) have good electrical conductivity but have high surface energy. They tend to easily

ISSN 2734-9381
https://doi.org/10.51316/jst.177.etsd.2024.34.4.6
Received: Mar 22, 2024; revised: Jun 22, 2024;
accepted: Jun 27, 2024.

agglomerate to form nanoclusters, reducing their surface area and electrocatalytic ability [7]. Graphene nanoplatelets (GNPs) have a large surface area, good electrical conductivity, and help stabilize iron-based nanomaterials [8]. In particular, immobilizing Fe on graphene improves the stability of Fe by preventing its aggregation, increasing the specific area, and thus facilitating electron transfer in Fe. Therefore, Fe/GNPs is improved and increase electrocatalytic efficiency for sensor applications. With the ability to bond and conduct electrons, Tetrakis (4-carboxyphenyl) porphyrin (TCPP) is added to increase the electrical conductivity and connection between the active material (Fe/GNPs) together and active material with the electrode surface [9]. As a result, Fe/GNPs/TCPP nanocomposite material was proved to be a potential material for application as an electrochemical sensor for the analysis of NFT antibiotic residues.

In this study, the NFT antibiotic detection capability of iron/graphene nanocomposite is presented. The green chemical method with CO extract is used as the reducing agent to synthesize Fe/GNPs and combined with TCPP to form Fe/GNPs/TCPP nanocomposite material with the self-assembled method. The morphology and structure of the material were characterized by Scanning Electron Microscope combined with Energy Dispersive X-ray Spectroscopy elemental mapping (SEM-EDX mapping), Fourier-transform infrared spectroscopy (FT-IR). The electrochemical properties as well as the NFT detection capability of the Fe/GNPs/TCPP coated electrode were confirmed by electrochemical measurement techniques including cyclic voltammetry (CV) and differential pulse voltammetry (DPV).

2. Experimental Method

2.1. Chemicals

In this study, the chemicals used were $FeCl_3.6H_2O$ (greater than 99%), $K_3Fe(CN)_6/K_4Fe(CN)_6$ (greater than 99%), and ethanol (99.7%) purchased from Xilong Science Ltd. NFT of 99% purity was supplied by Merklin. PBS buffer (pH equal 7.4) was prepared with NaCl, KCl, $Na_2HPO_4.12H_2O$, and KH_2PO_4 acquired from Xilong Science Ltd. Cleistocalyx Operculatus (CO) extract was synthesized according to published procedures [10]. 5 g of dried CO powder was stirred in 30 mL of ethanol for 2 hours at 50-60 ^oC. This mixture was filtered to obtain CO extract. CO leaf extract contains polyphenols, flavonoids, vitamins, and some major minerals with relatively high proportions of flavonoids (14%) and polyphenols (0.7%) for use as green reductants [10, 11]. The reducing agent solution used in this study was prepared by diluting CO extract in distilled water at a ratio of 1:20 in weight. Graphene nanoplatelets solution was provided by VNgraphene Joint Stock Company. Double distilled water was used throughout the entire experiment.

2.2. Synthesis of Fe/GNPs/TCPP

Fe/GNPs nanocomposite material was synthesized by the green chemistry method. A solution mixture of 0.025 g $FeCl_3$ and 5.6 mL graphene solution was dispersed in water by sonication, then transferred into a reaction vessel and placed on a magnetic stirrer at a speed of 300 rpm. 90 mL of Cleistocalyx Operculatus extract was slowly dropped into the reaction vessel to reduce Fe^{3+} to zero-valent iron nanoparticles. The obtained Fe/GNPs material was obtained, filtered, and centrifuged several times with ethanol, and subsequently dried under vacuum condition at 60 °C for 12 hours. The prepared Fe/GNPs samples were dispersed in TCPP, which was previously dissolved in 0.1 M NaOH. Afterward, the whole mixture was neutralized with 0.1 M HCl until the pH changed from 10 to 6.

2.3. Preparation of Working Electrode

The glassy carbon electrode (GCE, Metrohm) was surface treated with wet sandpaper, then rinsed thoroughly with distilled water. The prepared sample of Fe/GNPs/TCPP nanocomposite material was coated with 8 µL using the drop-casting method on the GCE surface and allowed to dry at ambient temperature.

2.4. Electrochemical Analysis

Electrochemical measurements were performed on an Autolab AUT86590 instrument (Metrohm) with a three-electrode system including a GCE (working electrode), a Pt mesh (counter electrode) and a Calomel electrode (reference electrode). The electrochemical behaviors of Fe/GNPs/TCPP material utilized in detection of NFT were investigated by cyclic voltammetry (CV) and differential pulse potential (DPV) in PBS buffer solution containing 200 µM NFT. CV measurements were conducted over a potential range of -1.1 V to 0 V with a scan rate of 50 mV/s. DPV measurements were carried out under the following parameters: $E_{pulse} = 0,075\ V$, $T_{pulse} = 0,2s$, $scan\ rate = 6\ mVs^{-1}$, potential ranged from -0,2 V to -0,6 V.

2.5. Characterization of Materials

The morphology, grain size, and elemental composition of materials were investigated using a scanning electron microscope with X-ray energy dispersive spectroscopy (SEM-EDX) on a Hitachi S-4600 instrument. The Brucker Cave Tensor II FT-IR spectroscopy device is used to record the vibrations of chemical bonds in the structure of materials, with a measuring range of 400 cm^{-1} to 4000 cm^{-1}.

2.6. Analysis Capability Comparison

NFT solutions with concentrations of 1, 5, 10, 20, 50, 100, and 150 µM were prepared for UV-Vis analysis at 363 nm wavelength on a Shimadzu UV-1800 instrument.

3. Results and Discussion

3.1. Characterization of the Fe/GNPs/TCPP Nanocomposite

The morphology of Fe/GNPs/TCPP nano-composite was evaluated by SEM and the results are shown in Fig. 1. Fig. 1a shows a sample of Fe/GNPs nanocomposite material with a microscopic size of approximately 30-50 nm evenly distributed on the surface of GNP sheets to form sheets of nanocomposite material.

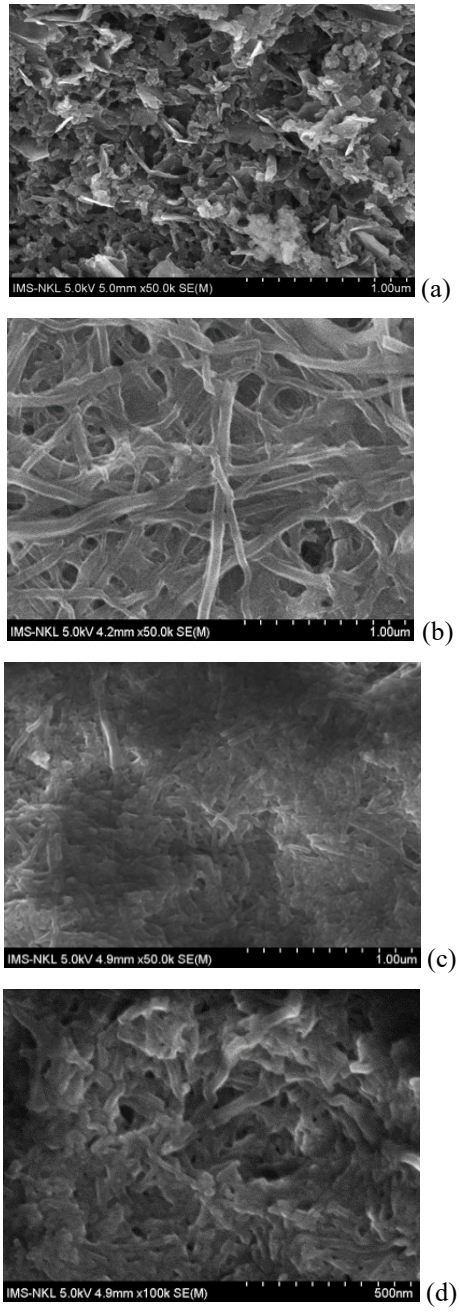

Fig. 1. SEM results of (a) Fe/GNPs; (b) TCPP nanofibers; (c, d) Fe/GNPs/TCPP

The morphology of the self-assembled TCPP has been demonstrated in Fig. 1b, showing the structure of TCPP filaments of about 20 nm in diameter and several μm in length. Fig. 1c and Fig. 1d show the combination of Fe/GNPs and TCPP. It is clear that the Fe/GNPs composite is evenly distributed and interspersed in the TCPP fiber network, indicating the favorable formation of Fe/GNPs/TCPP materials.

The chemical bonding properties of the material were investigated using FT-IR, as depicted in Fig. 2. The FT-IR spectrum of Fe/GNPs/TCPP exhibits a broad vibrational spectrum with a center at about 3317 cm^{-1}. This characteristic wavelength is due to the distinctive vibration of the -OH bond originating from the polysaccharide carbonyl groups present in the extract, as well as the water molecules that have been absorbed [12]. The peaks observed at 1697 cm^{-1} and 1640 cm^{-1} are assigned to the vibrations of C=O and C-N in organic compounds [13]. These results reflect the fact that the surface of the Fe/GNPs nanocomposite was coated with a protective layer consisting of naturally derived polysaccharide components from CO extract. The absorption peak observed at wavenumber 549 cm^{-1} is attributed to the Fe–O stretching phenomenon exhibited by iron nanoparticles [14]. The FT-IR spectrum of the porphyrin nanostructure shows absorption bands at wavenumbers of 1638 cm^{-1} and 1401 cm^{-1}, which may be due to the binding of C=O and C-O groups in the TCPP molecule [15]. FT-IR spectra has confirmed the successful formation of Fe/GNPs/TCPP composite without any chemical interactions between these components.

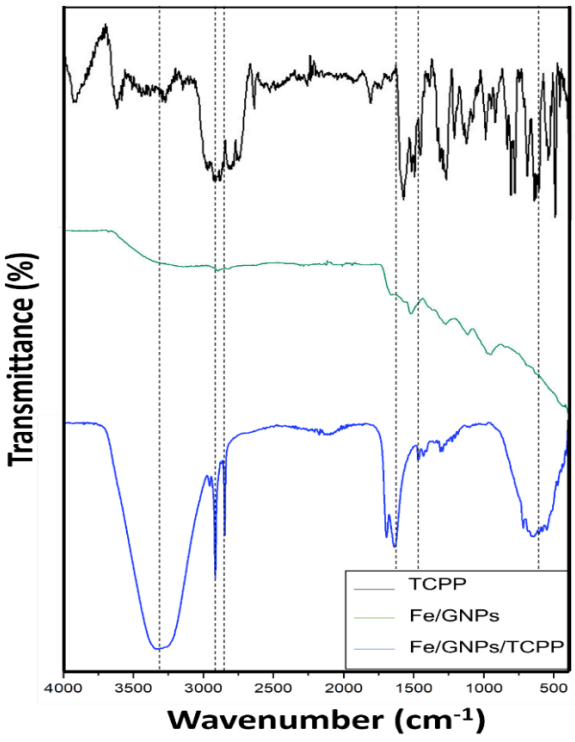

Fig. 2. FT-IR spectra of TCPP nanofibers, Fe/GNPs, and Fe/GNPs/TCPP nanocomposites

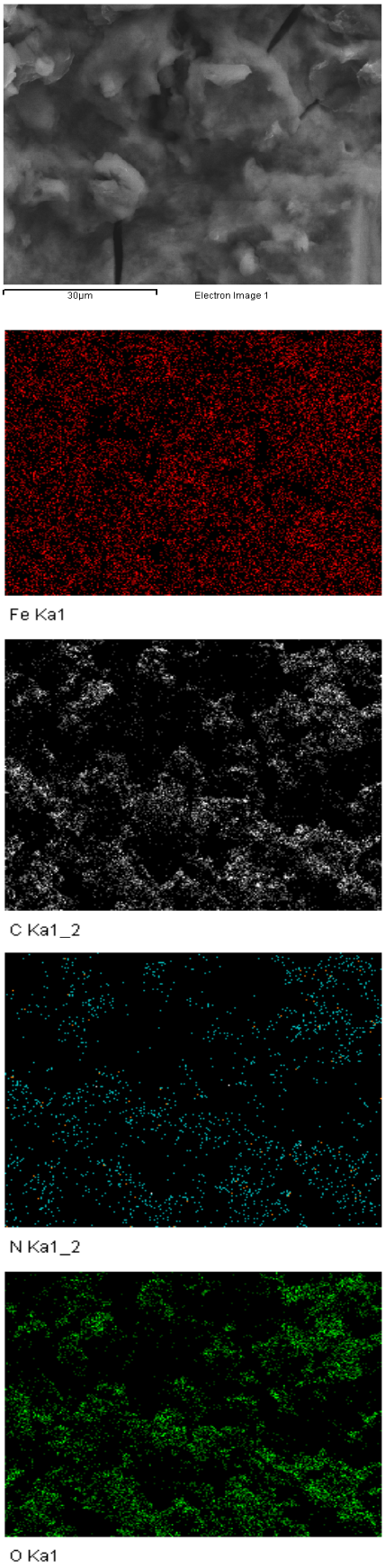

Fig. 3. EDX-mapping analysis results of Fe/GNPs/TCPP nanocomposite materials

3.2. Application of Fe/GNPs/TCPP in NFT Detection Sensor

3.2.1. Detection of NFT in solution capability

The sensing capability of the GCE modified with Fe/GNPs/TCPP material was investigated by CV scanning in solutions without and containing 200 µM NFT. The results are shown in Fig. 4.

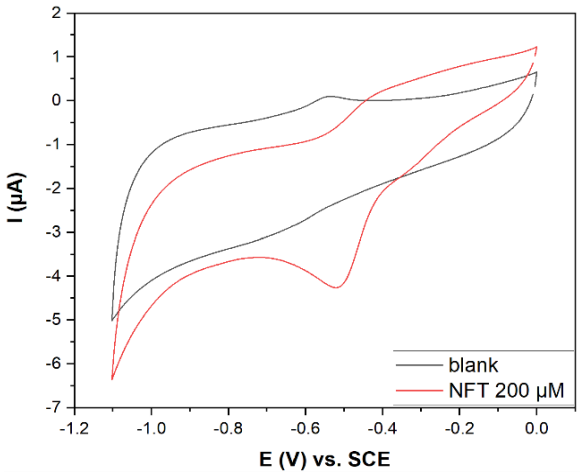

Fig. 4. CV curves of Fe/GNPs/TCPP material on GCE in solutions containing and without NFT

In the blank solution, the CV curve does not demonstrate the distinctive peak of the reduction reaction in the potential ranging from -1.1 V to 0 V. However, with the presence of NFT in solution at 200 µM, the characteristic peak of the reduction reaction of NFT to produce -NO_2 is clearly witnessed at the potential of -0,52 V on the CV curve. The reduction reaction of NFT is carried out according to the equation below:

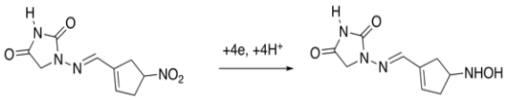

(1)

The results have confirmed that the GCE coated with Fe/GNPs/TCPP material is capable of detecting NFT in solution.

3.2.2. The influence of scan rate

Kinetics of the reaction was studied through scan rate. The influence of different scan rates on NFT detection was performed using CV measurements. Fig. 5 shows the CV curves of Fe/GNPs/TCPP material on a GCE in a solution containing 100 µM NFT with scan rates ranging from 10 to 100 mV/s. The signal intensity of the response current rose with increasing scan rate, and the reaction potential shifted to a more positive direction, indicating that the reaction occurred more easily. When the scan rate increased from 10 mV/s to 100 mV/s, the reduction peak intensity improved linearly according to the function: $y = 0,0215x + 1,4665$ with a high correlation coefficient (R^2) of 0,9697 (in Fig. 6). It implied that the

electrochemical reaction of NFT on the electrode surface was controlled by the adsorption process. This explanation has been discussed by different publications [16]. The shell layer on the Fe surface has a porous structure, and GNPs has a large surface area and active sites. Therefore, NFT molecules may adsorb to those positions. First, NFT and the surface have an electrostatic interaction force, and then an electron exchange reaction will occur on the working surface. Since the response current is proportional to the scan rate, as the scanning speed increases, the response current becomes higher. However, when the scan rate is too high, NFT molecules do not have time to perform the reduction reaction on the electrode surface. Therefore, a scan rate of 50 mV/s was chosen, which corresponds to many other references [17].

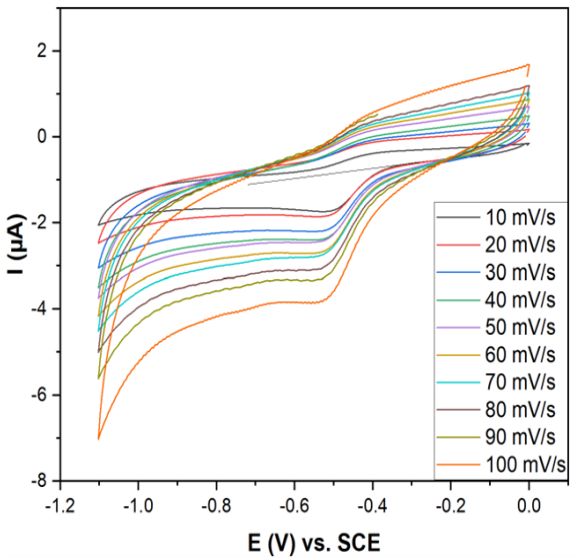

Fig. 5. CV curves of 100 µM NFT at different scan rates

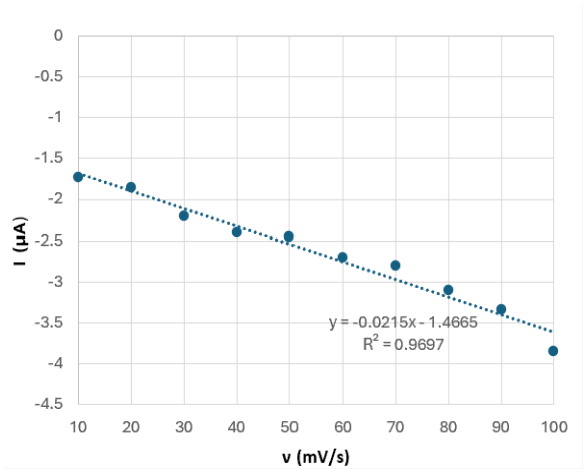

Fig. 6. Linear plot showing correlation between response current and scan rate

3.2.3. The influence of material loading amount

The electrode surface is the most important in electrochemical sensors. Therefore, the influence of Fe/GNPs/TCPP material amounts loaded onto the electrode was investigated at different quantities (2, 4, 6, 8 µL) (Fig. 7 and Fig. 8). When the amount of material increased from 2 to 4 µL, the response current rose rapidly (from 1.625 µA to 4.371 µA). Surprisingly, the response current dropped sharply as the amount of material went from 4 to 8 µL. With the amount of Fe/GNPs/TCPP material being 4 µL, the capability to transfer electrons to the electrode surface for the reduction reaction was the most effective. Therefore, 4 µL of Fe/GNPs/TCPP was selected for further investigation.

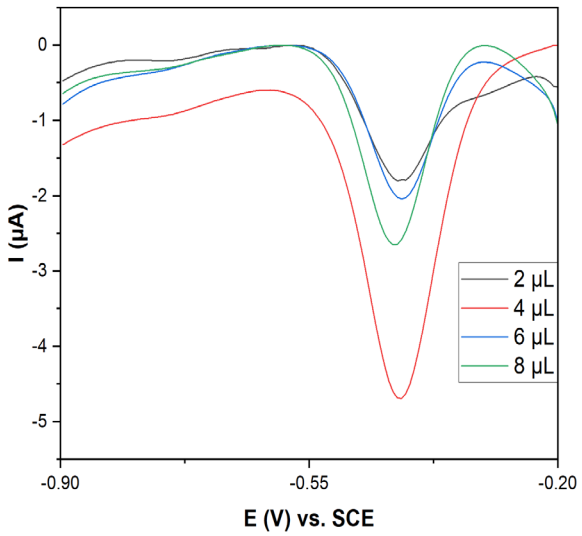

Fig. 7. The effect of loading material of Fe/GNPs/TCPP in 200 µM of NFT

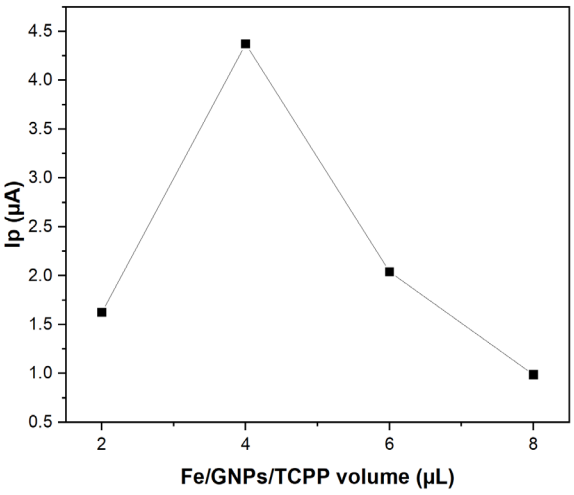

Fig. 8. Effect of material amount on NFT response current

3.2.4. The influence of pH

pH is an important parameter that affects the ability of NFT reduction reaction to occur. The effect of pH between 3 and 11 was investigated in a solution containing 200 µM of NFT (Fig. 9 and Fig. 10). DPV measurement results show that the response current signal gradually increased as pH went up from 3 to 7 and gradually decreased when pH was greater than 7. This could be explained by the fact that in acidic environments, the number of H^+ in the solution is higher, which allows NFTs to be reduced more easily, resulting in higher response currents than those in alkaline environments. Therefore, pH equal 7 was chosen for other surveys.

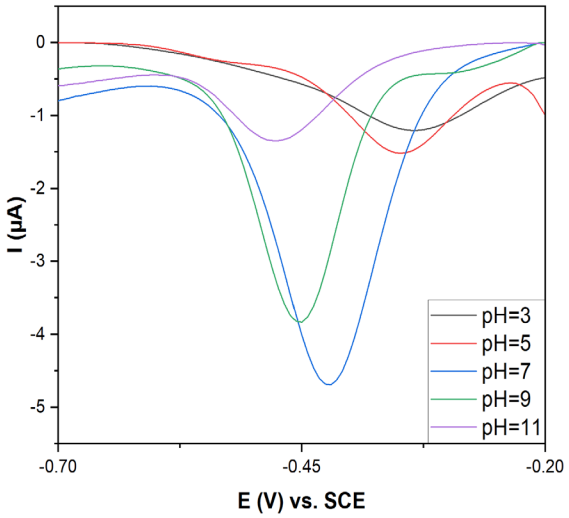

Fig. 9. DPV profile of 200 µM NFT at varying pH values of 3, 5, 7, 9, 11

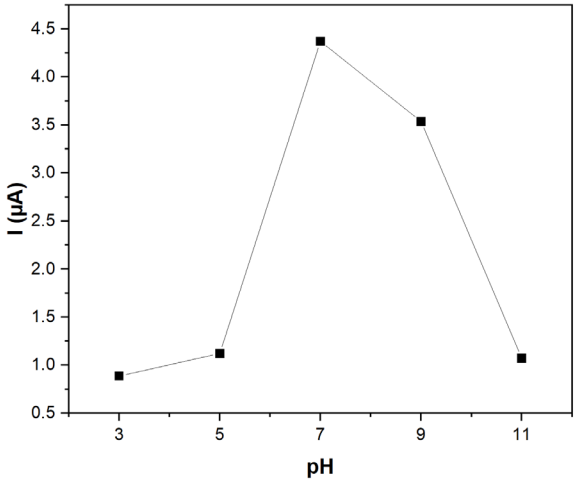

Fig. 10. Calculated response current of 200 µM NFT at different pH

3.2.5. Calibration curve for NFT detection sensor

The standard curve of the electrochemical sensor detecting NFT was built in the concentration range between 1 µM and 200 µM. Solution with different NFT concentrations of 1, 40, 100, 150, and 200 µM were prepared for DPV analysis in the potential range from -0.2 V to -0.6 V with a scan rate of 50 mV/s at pH equal 7. The DPV curve is shown in Fig. 11. The graph demonstrates that the response current intensity increased as the NFT concentration in the solution was higher. The current intensity responds linearly to NFT concentration according to a first-order function: $y=0,0153x + 0,0417$ $(R^2=0,9987)$ (Fig. 12).

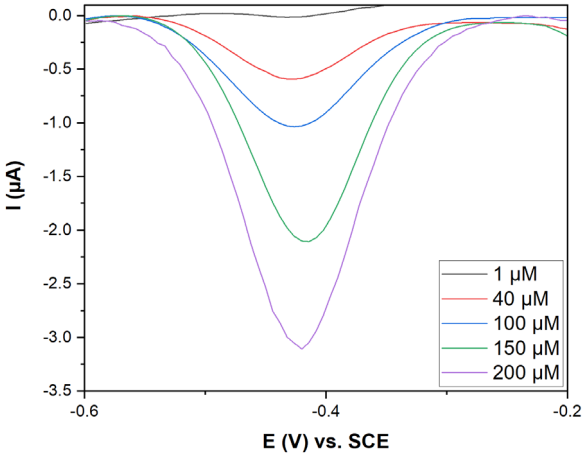

Fig. 11. DPV response current of Fe/GNPs/TCPP with various concentrations of NFT

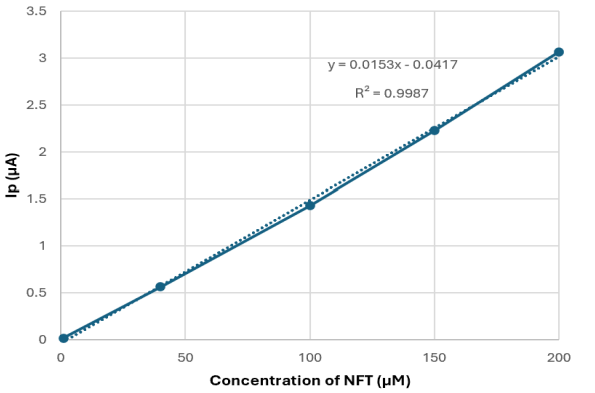

Fig. 12. Relationship between response current and NFT at different concentrations

Some previous studies on electrochemical sensor materials to detect NFT have been reported. CeO_2 nanocomposite material has been to detect NFT with limit of detection (LOD) of 7.81 µM and linear range of 20 ÷ 100 µM while nanocomposite NiO/BCN has a LOD of 10 µM; sensitivity of 1.15 $\mu A.\mu M^{-1}.cm^{-2}$ and linear range of 0.05 ÷230 µM [18, 19]. In this study, the Fe/GNPs/TCPP nanocomposite material achieved the LOD value of 0.504 µM with sensitivity of 0.9421 $\mu A.\mu M^{-1}.cm^{-2}$ and linear range of 1÷200 µM. This material gives the lower LOD and relatively good sensitivity compared to other materials in NFT detection. Research data shows that Fe/GNPs/TCPP has potential for application in detecting NFT antibiotic residues.

The experiment to compare the capability of detecting NFT between the electrochemical analysis method and conventional method (UV-Vis in this case) was carried out and presented in Fig. 13 and Fig. 14.

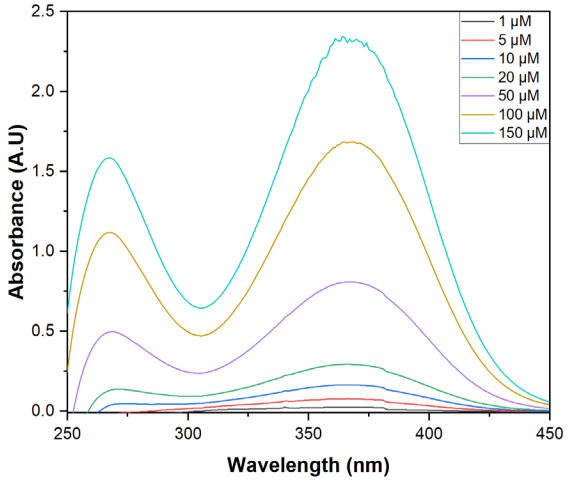

Fig. 13. Results of UV-Vis analysis of NFT solution at 363 nm wavelength

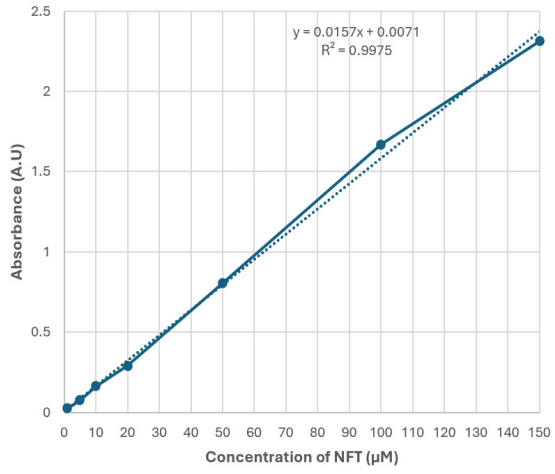

Fig. 14. Calibration of absorbance at various concentrations of NFT.

It can be seen that the electrochemical method provided higher sensitivity and better accuracy over a wider linear range (at 200 µM in this study) than UV-Vis analysis. The UV-Vis analysis method works preferably at concentrations of less than 150 µM. If the concentration is higher than this point, the UV-Vis device will not be able to operate accurately since it produces significant noises.

4. Conclusion

Using the green synthesis method combined with the self-assembled method, Fe/GNPs/TCPP nanocomposite material had been successfully synthesized. Modern characterization methods showed that the synthesized iron nanoparticles with a size of 30 nm to 50 nm, had been evenly distributed on the surface of the GNPs sheets and were interspersed in the TCPP fibers. Fe/GNPs/TCPP nanocomposite exhibited good electrochemical properties for the capability to detect the NFT antibiotic in solution. The electrochemical behavior of NFT was controlled by its adsorption onto the electrode surface. At pH equal 7 and the material loading amount of 4 µL, the NFT reduction reaction gave the most significant response current signal and produced a standard curve with a wide linear range (1 µM to 200 µM) for NFT detection. These results will be an important premise for applications of Fe/GNPs/TCPP nanocomposite materials in electrochemical sensors to detect antibiotic residues in agricultural products.

Acknowledgments

The authors gratefully acknowledge the financial support of the Asahi Glass Foundation (No: AGF. 2023-02).

References

[1] A. Saini, M. Kumar, S. Bhatt, V. Saini, and A. Malik, Cancer causes and treatments, Int. J. Pharm. Sci. Res., vol. 11, no. 7, Jul. 2020, pp. 3121-3134. https://doi.org/10.13040/IJPSR.0975-8232

[2] M. M. J. Arsène *et al.*, The public health issue of antibiotic residues in food and feed: Causes, consequences, and potential solutions, Veterinary World, vol. 15, no. 3, Mar. 2022, pp. 662-671. https://doi.org/10.14202/vetworld.2022.662-671

[3] K.-Y. Hwa and T. S. K. Sharma, Nano assembly of NiFe spheres anchored on f-MWCNT for electrocatalytic reduction and sensing of nitrofurantoin in biological samples, Sci. Rep., vol. 10, no. 1, Jul. 2020, pp. 12256. https://doi.org/10.1038/s41598-020-69125-5

[4] Y. Sun, G. I. N. Waterhouse, X. Qiao, J. Xiao, and Z. Xu, Determination of chloramphenicol in food using nanomaterial-based electrochemical and optical sensors-A review, Food Chem., vol. 410, Jun. 2023, pp. 135434. https://doi.org/10.1016/j.foodchem.2023.135434

[5] N. V. Hoang *et al.*, Green synthesis of Fe/Graphene nanocomposite using Cleistocalyx operculatus leaf extract as a reducing agent: removal of pollutants (RhB dye and Cr6+ ions) in aqueous media, ChemistrySelect, vol. 7, no. 47, Dec. 2022, pp. e202203499, . https://doi.org/10.1002/slct.202203499

[6] S. Xiao *et al.*, Polyelectrolyte multilayer-assisted immobilization of zero-valent iron nanoparticles onto polymer nanofibers for potential environmental applications, ACS Appl. Mater. Interfaces, vol. 1, iss. 12, Dec. 2009, pp. 2848-2855. https://doi.org/10.1021/am900590j

[7] D. Vollath, Agglomeration of particles stored in a box, FirePhysChem, vol. 3, iss. 3, Sep. 2023, pp. 275-280. https://doi.org/10.1016/j.fpc.2023.03.007

[8] Q. Wan *et al.*, Graphene nanoplatelets: electrochemical properties and applications for oxidation of endocrine-disrupting chemicals, Chem. - Eur. J., vol. 19, no. 10, Jan. 2013, pp. 3483-3489. https://doi.org/10.1002/chem.201203607

[9] D. D. La *et al.*, Self-assembly of monomeric porphyrin molecules into nanostructures: Self-assembly pathways and applications for sensing and environmental treatment, Environ Technol Invo., vol. 29, Feb. 2023, pp. 103019. https://doi.org/10.1016/j.eti.2023.103019

[10] T. H. Nguyen *et al.*, Green synthesis of a photocatalyst Ag/TiO2 nanocomposite using Cleistocalyx operculatus leaf extract for degradation of organic dyes, Chemosphere, vol. 306, Nov. 2022, pp. 135474. https://doi.org/10.1016/j.chemosphere.2022.135474

[11] K. H. Le *et al.*, Fabrication of Cleistocalyx operculatus extracts/chitosan/gum arabic composite as an edible coating for preservation of banana, Prog. Org. Coat., vol. 161, Dec. 2021, pp. 106550. https://doi.org/10.1016/j.porgcoat.2021.106550

[12] M. K. Medlej *et al.*, Antioxidant activity and biocompatibility of fructo-polysaccharides extracted from a wild species of Ornithogalum from Lebanon, Antioxidants, vol. 10, no. 1, Jan. 2021, pp. 68. https://doi.org/10.3390/antiox10010068

[13] V. G. Gregoriou, V. Jayaraman, X. Hu, and T. G. Spiro, FT-IR Difference spectroscopy of hemoglobins A and Kempsey: Evidence that a key quaternary interaction induces protonation of Asp. beta. 99, Biochem., vol. 34, no. 20, May. 1995, pp. 6876-6882. https://doi.org/10.1021/bi00020a035

[14] M. Rengasamy, K. Anbalagan, S. Kodhaiyolii, and V. Pugalenthi, Castor leaf mediated synthesis of iron nanoparticles for evaluating catalytic effects in transesterification of castor oil, RSC Adv., vol. 6, no. 11, Jan. 2016, pp. 9261-9269. https://doi.org/10.1039/C5RA15186D

[15] D. D. La, S. V. Bhosale, L. A. Jones, N. Revaprasadu, and S. V. Bhosale, Fabrication of a Graphene@ TiO2@ Porphyrin hybrid material and its photocatalytic properties under simulated sunlight irradiation, ChemistrySelect, vol. 2, no. 11, Apr. 2017, pp. 3329-3333. https://doi.org/10.1002/slct.201700473

[16] B. Karuppaiah, R. Ramachandran, S.-M. Chen, S. Wan-Ling, and J. Y. J. N. J. o. C. Wan, Hierarchical construction and characterization of lanthanum molybdate nanospheres as an unassailable electrode material for electrocatalytic sensing of the antibiotic drug nitrofurantoin, New J. Chem., vol. 44, no. 1, Nov. 2020, pp. 46-54. https://doi.org/10.1039/C9NJ05347F

[17] P. Balasubramanian, M. Annalakshmi, S.-M. Chen, T. Sathesh, and T. S. T. Balamurugan, Ultrasonic energy-assisted preparation of β-cyclodextrin-carbon nanofiber composite: Application for electrochemical sensing of nitrofurantoin, Ultrason. Sonochem., vol. 52, Apr. 2019, pp. 391-400. https://doi.org/10.1016/j.ultsonch.2018.12.014

[18] H. A. Rudayni, A. A. Chaudhary, G. M. Abu-Taweel, M. Shariq, and M. Imran, Hydrothermal synthesis of CeO2 nanoparticles and its application in electrochemical detection of nitrofurantoin antibiotics, Europhys. Lett., vol. 137, no. 6, May. 2022, pp. 66005. https://doi.org/10.1209/0295-5075/ac6065

[19] T. Kokulnathan and T.-J. Wang, Synthesis and characterization of 3D flower-like nickel oxide entrapped on boron doped carbon nitride nanocomposite: An efficient catalyst for the electrochemical detection of nitrofurantoin, Compos. B Eng., vol. 174, Oct. 2019, pp. 106914. https://doi.org/10.1016/j.compositesb.2019.106914